Journal of Power Sources 239 (2013) 374–381

Contents lists available at SciVerse ScienceDirect

Journal of Power Sources

journal homepage: www.elsevier.com/locate/jpowsour

Surfactant-free synthesis of highly methanol-tolerant, polyhedral Pd–Pt nanocrystallines for oxygen reduction reaction

Yongfu Tang*, Faming Gao, Shengxue Yu, Zhiping Li, Yufeng Zhao

Key Laboratory of Applied Chemistry, Yanshan University, Qinhuangdao, Hebei 066004, China

HIGHLIGHTS

- Polyhedral Pd–Pt nanocrystallines were synthesized without any surfactants.
- Low-Pt polyhedral Pd–Pt/C catalysts exhibit comparable ORR to TKK Pt/C catalyst.
- The as prepared Pd–Pt/C show excellent methanol tolerance.
- Polyhedral Pd–Pt/C with low ECSA show 1.56-fold mass activity to spherical Pd–Pt/C.

GRAPHICAL ABSTRACT

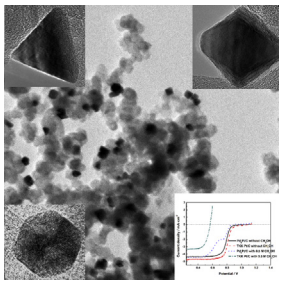

ARTICLE INFO

Article history:
Received 29 December 2012
Received in revised form
25 March 2013
Accepted 26 March 2013
Available online 6 April 2013

Keywords:
Polyhedral nanocrystalline
Low platinum catalysts
Palladium–platinum catalysts
Oxygen reduction reaction
Surfactant-free synthesis
Methanol tolerance

ABSTRACT

Carbon supported polyhedral Pd–Pt nanocrystallines (Pd–Pt/C) are synthesized using a facile surfactant-free process. The morphology of nanocrystallines is tailored by ammonia complexation and Pd/Pt ratios of the metallic precursors. The as-prepared Pd–Pt/C catalysts with low Pt content exhibit oxygen reduction reaction (ORR) activity comparable to that of the commercial Pt/C catalyst, while having much higher methanol tolerance. Compared with the spherical Pd_6Pt/C catalyst, the polyhedral Pd_6Pt/C catalyst shows 1.56-fold higher mass specific activity for ORR, while its electrochemical surface area (ECSA) is only half of the former. The superior ORR activity may be attributed to the more exposed regular (111) planes, the higher ratio of metallic form and the surface enrichment of Pt atoms.

1. Introduction

Direct methanol fuel cells (DMFCs) have attracted great interest as portable power sources due to their high energy density, low operating temperature and available fuel [1]. Pt-based catalysts, with high catalytic activity for oxygen reduction reaction (ORR) and high stability, are widely used as the cathode catalysts for DMFCs [2]. However, the high cost of platinum and the methanol poisoning on platinum caused by the crossover of methanol hinder the commercialization of DMFCs. The permeation of methanol from the anode to the cathode through membrane leads to significant deterioration of cathode performance by poisoning the Pt catalyst and causes a mixed potential [3].

Pd-based catalysts have been regarded as one of the most promising cathode catalysts for DMFCs due to their similar activities for ORR and superior methanol tolerance to the commercial Pt/C catalysts. Adzic et al. [4] reported that the Pd_3Fe/C catalyst showed higher activity for ORR than the commercial Pt/C catalyst.

* Corresponding author. Tel.: +86 13780351724.
E-mail address: tangyongfu@ysu.edu.cn (Y. Tang).

0378-7753/$ – see front matter © 2013 Elsevier B.V. All rights reserved.
http://dx.doi.org/10.1016/j.jpowsour.2013.03.151

Pd–Co–Au and Pd–Ti catalysts [5] also exhibited comparable catalytic activity for ORR to that of commercial Pt catalyst. However, the chemical and electrochemical stability of Pd-based catalysts alloying with transition metals (Fe, Co, Ni) is inferior due to the dissolution of transition metals. Pd–Pt bimetallic catalysts [6–8], especially those shape-controlled nanophases, have attracted more attention due to their high activity for ORR, high stability and excellent methanol tolerance. Shape-controlled Pd and Pt nanoparticles with polyhedral structures, including tetrahedral, cubic, octahedral, twinned nanoparticle and so on exhibit higher activity, owing to their more regular planes [8–10]. Lee et al. reported that tetrahedral and octahedral Pd–Pt nanocrystallines, which have more regular (111) planes exposed, exhibit enhanced activity and stability for ORR [8]. However, in the synthesis of the shape controlled Pd-based nanoparticles, surfactants (e.g., CTAB [11], PVP [12,13]) are usually used as stabilizer to prevent the aggregation and shape distortion of the Pd nanoparticles. These surfactants are strongly adsorbed on the particle surface and difficult to remove completely, which would markedly reduce the active sites for the electrocatalytic reaction. Therefore, facile processes without surfactants are highly desirable to produce nanoparticles with well-defined shapes for improved electrochemical catalysis.

Herein, we report a facile route without surfactants for the synthesis of carbon supported Pd–Pt catalysts with tetrahedral, octahedral and 5-fold twinned structures. In this process, the reduction kinetics of metal precursor was tailored by complexing the metal ion with ammonia and controlling the Pd/Pt atomic ratios. The reduction kinetics and the adsorption of ammonia on the surface of nanoparticles play key roles in the shape control of metal nanoparticles. The morphologies of polyhedral nanoparticles were characterized by transmission electron microscopy (TEM) and high-resolution transmission electron microscopy (HRTEM). Electrochemical measurements were performed using cyclic voltammetry (CV) by rotating disk electrode (RDE) to investigate the structure-dependent ORR and methanol oxidation reaction (MOR) activities of the as prepared Pd–Pt/C catalysts. The surface structure and composition of Pd–Pt/C catalysts were measured by HRTEM and X-ray photoelectron spectroscopy (XPS) to investigate their effects on the catalytic activities of Pd–Pt/C catalysts.

2. Experimental

2.1. Catalysts preparation

A series of carbon supported polyhedral Pd–Pt catalysts with low Pt content was prepared by a modified ethylene glycol method. The ammonia solution was used as complexing reagent, and ammonia gas carried by nitrogen was used as protective gas. Various amounts of H_2PdCl_4 solution (dissolved $PdCl_2$ in the hydrochloride acid) were mixed with 40 mL ethylene glycol. Excess ammonia solution was added until the yellow solution became colorless, indicating the formation of the Pd–NH_3 complex. The designated amount of H_2PtCl_6 dissolved in the ethylene glycol was added in the solution, followed by the addition of 70 mg Vulcan XC-72 carbon black dispersed in 20 mL ethylene glycol. The mixture was heated in an oil bath at 130 °C for 3 h with $NH_3 + N_2$ as protective gas. After cooling and aging, the mixture was centrifuged, washed and dried. The Pd/Pt atomic ratios were 9:1, 6:1 and 4:1, respectively, and the obtained catalysts are denoted as Pd_9Pt/C–NH_3, Pd_6Pt/C–NH_3 and Pd_4Pt/C–NH_3.

To further investigate the role of ammonia gas on the morphologies of nanoparticles, the Pd_6Pt/C catalyst was prepared by the method similar to Pd_6Pt/C–NH_3 with ammonia solution as complexing reagent, but only with N_2 as protective gas for comparison. The as-prepared catalyst was denoted as Pd_6Pt/C–NH_3–N_2.

The third Pd_6Pt/C catalyst was prepared in the absence of ammonia during the whole preparation process (ammonia solution was not used as a complexing reagent and NH_3 was not used as a protective gas) for comparison. The as-prepared catalyst was denoted Pd_6Pt/C–EG. Moreover, the metal loading of all the catalysts in this study was 30% in weight.

2.2. Physicochemical characterizations

Powder X-ray diffraction (XRD) analyses of Pd–Pt/C and Pt/C catalysts were conducted with PANalytical X'Pert-Pro powder X-ray diffractometer using Ni-filtered Cu Kα radiation (λ = 1.54056 Å). The XRD patterns were recorded over a 2θ range of 10–90° at the step size of 0.033°. The average crystallite sizes of the catalysts were evaluated by the Scherrer formula [14,15]:

$$L = \frac{0.9\lambda_{K\alpha 1}}{B_{2\theta}\cdot\cos\theta_B} \quad (1)$$

where the L, $\lambda_{K\alpha 1}$, $B_{2\theta}$ and θ_B are the average crystallite sizes, the X-ray wave-length (1.54056 Å), the half-peak width of 2θ and the angle corresponding to the peak maximum, respectively.

Transmission electron microscope (TEM) images were recorded on a Tecnai G^2 Spirit (FEI Corp.) microscope operating at 120 kV. High resolution transmission electron microscope (HRTEM) images were performed on a TECNI F30 field emission electron microscope with acceleration voltage of 300 kV. The catalyst was placed in a vial containing ethanol and ultrasonically agitated to form homogeneous slurry. A drop of the slurry was dispersed on a holey amorphous carbon film on a Cu grid for analysis.

XPS spectra were obtained using a VG ESCALAB250 (Thermo VG Corp., USA) spectrometer equipped with Al-K_α resource (1486.6 eV, 15 kV, 10 mA). The base pressure of the system was $2*10^{-8}$ Pa, and the measurements were carried out at $2*10^{-7}$–$1*10^{-6}$ Pa. For each catalyst, a survey spectrum was collected before high resolution spectra were recorded. Deconvolutions of the XPS spectra were carried out using software XPS Peak 4.1.

2.3. Electrochemical measurements

Electrochemical measurements were conducted on the Power Suite 2273 electrochemical station (Princeton Corp. USA) with a rotate disk electrode (RDE) system (EG&G model 616). A standard three-electrode electrochemical cell was used as the measurement system. The as-prepared catalyst dispersed on the glassy carbon RDE was used as work electrode. A Pt foil (1 cm^2) and a saturated calomel electrode (SCE) were served as the counter electrode and the reference electrode, respectively. All the electrode potentials in this paper were quoted to normal hydrogen electrode (NHE). The metal loading on the RDE of all the electrochemical measurements is 0.114 mg cm^{-2}. Cyclic voltammetry (CV) measurements were conducted in high purity N_2 saturated 0.5 M H_2SO_4 solution, and carried out between 0.00 V and 1.20 V at the potential scan rate of 50 mV s^{-1}. The ORR activities were tested in O_2 saturated 0.5 M H_2SO_4 solution between 1.15 V and 0.24 V at the potential scan rate of 50 mV s^{-1}, with the RDE rotating at the speed of 1600 rpm. The methanol tolerance of catalysts was measured by testing the ORR in the O_2 saturated H_2SO_4 solution with 0.5 M methanol at a potential scan rate of 5 mV s^{-1}. To confirm the results of the methanol tolerance of the catalysts, the MOR curves were tested in the high purity N_2-saturated H_2SO_4 solution with 0.5 M methanol at a potential scan rate of 5 mV s^{-1}.

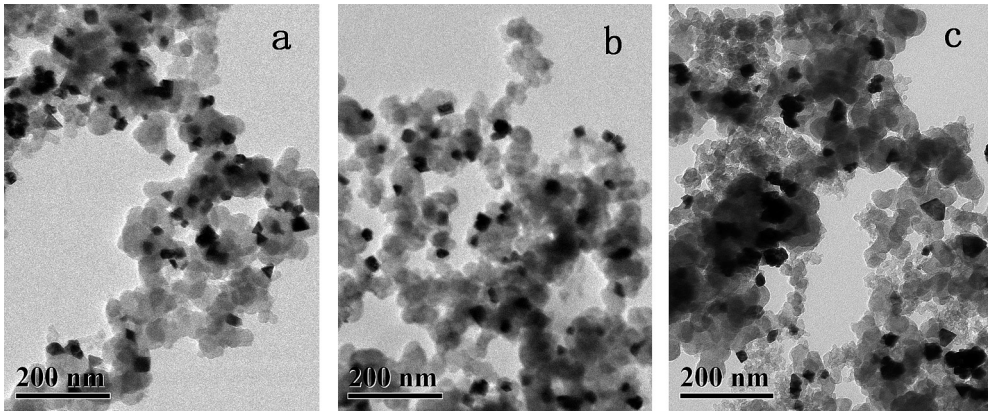

Fig. 1. TEM images of $Pd_9Pt/C–NH_3$ (a), $Pd_6Pt/C–NH_3$ (b) and $Pd_4Pt/C–NH_3$ (c) catalysts.

3. Results and discussion

3.1. Characterizations and evaluations of polyhedral Pd–Pt/C catalysts

Fig. 1 shows typical TEM images of the $Pd_9Pt/C–NH_3$, $Pd_6Pt/C–NH_3$ and $Pd_4Pt/C–NH_3$ catalysts. Tetrahedral and octahedron nanoparticles are observed in these samples. To the best of our knowledge, this is the first report for the preparation of Pd-based nanotetrahedron and nanooctahedron without any surfactants and polymers. Some aggregation appears in the image of the $Pd_4Pt/C–NH_3$ catalyst, and its particle size is larger than those of the other two Pd–Pt/C catalysts. The increased ratio of tetrahedral and octahedral nanoparticles in the $Pd_6Pt/C–NH_3$ image than for the other two Pd–Pt/C catalysts demonstrates that the Pd/Pt ratio is important for the formation of the polyhedral nanoparticles.

Fig. 2 shows the HRTEM images of the $Pd_6Pt/C–NH_3$ catalysts, where regular tetrahedral (Fig. 2b), octahedral (Fig. 2c) and 5-fold twinned (Fig. 2d) nanoparticles can be observed with a size of about 20 nm. Fig. 3 shows the TEM images and the electronic diffraction (fast Fourier transformation, FFT) patterns for their characteristic planes. The dominant planes of tetrahedral (Fig. 3a)

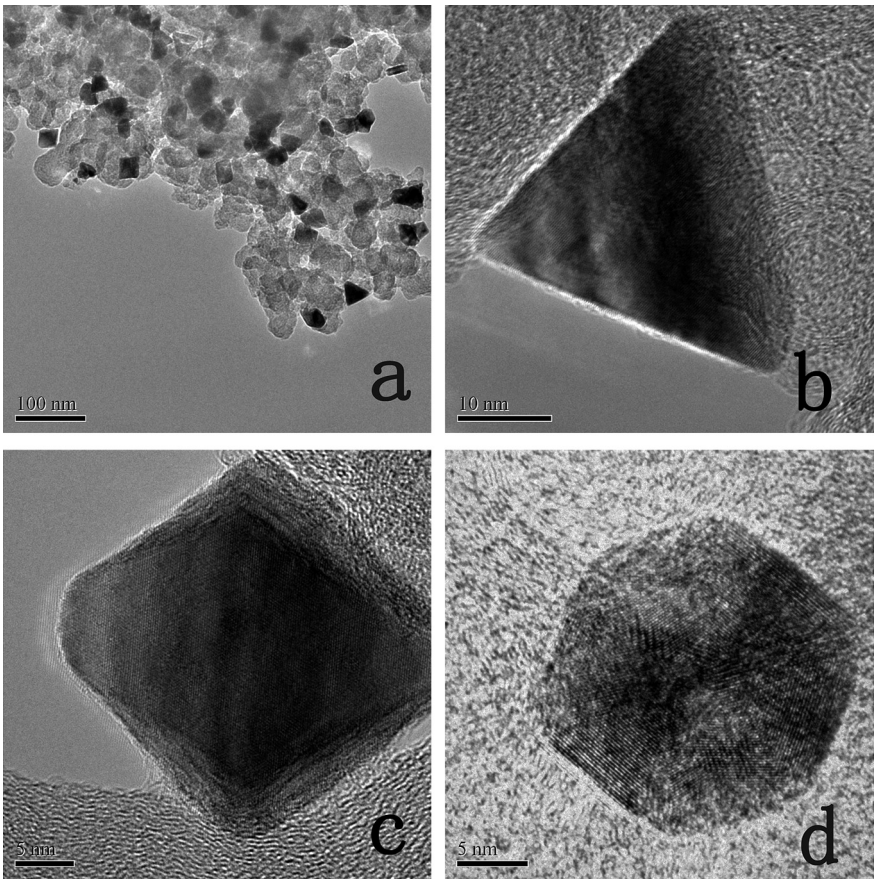

Fig. 2. HRTEM images of the different polyhedral nanoparticles on the $Pd_6Pt/C–NH_3$ catalysts: a) overview of HRTEM image, b) tetrahedral nanoparticle, c) octahedral nanoparticle and d) twinned structure nanoparticle.

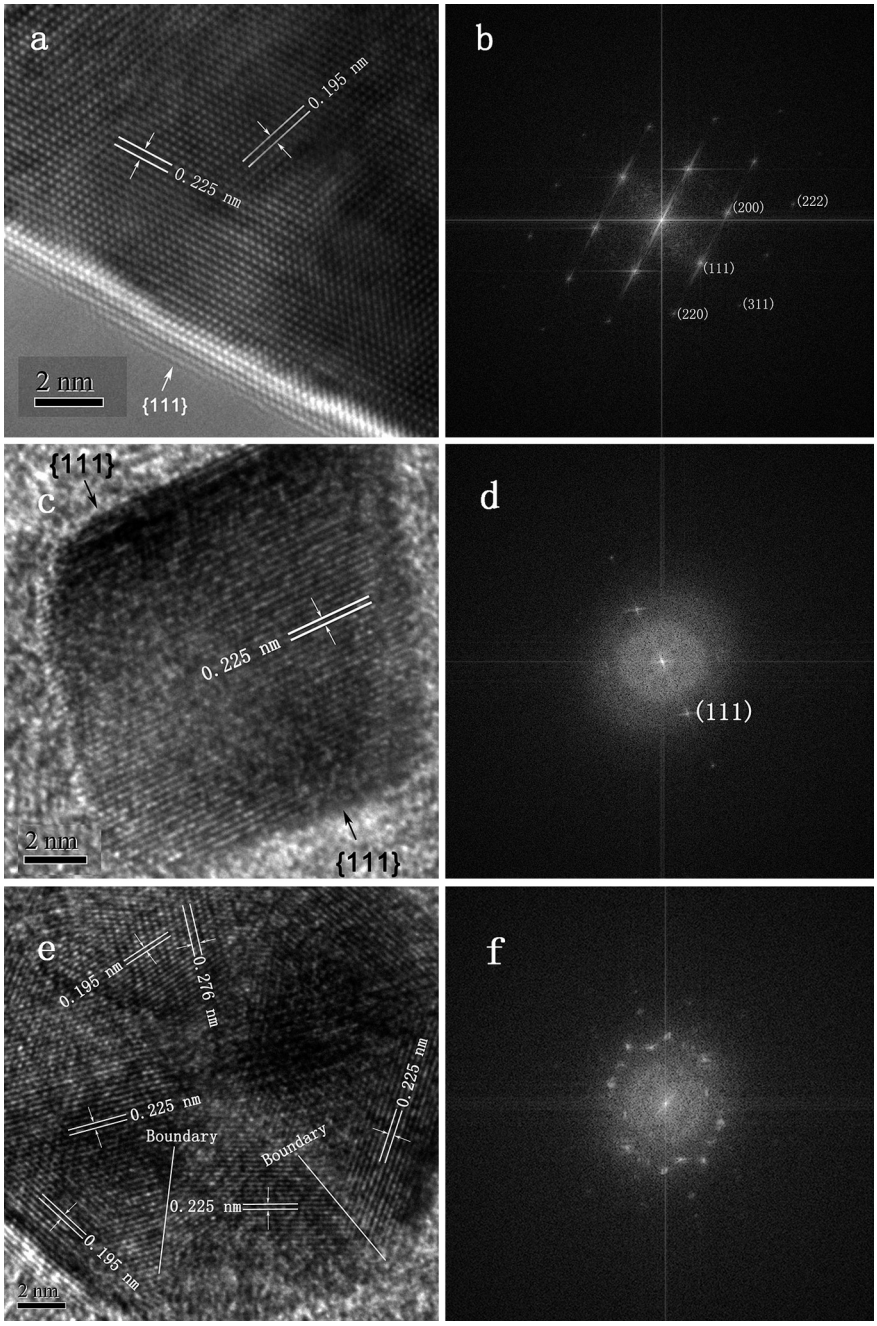

Fig. 3. Plane and FFT patterns of electronic diffraction in the $Pd_6Pt/C–NH_3$ catalyst: a), b) tetrahedral nanoparticle; c), d) octahedral nanoparticle; e), f) twinned structure nanoparticle.

and octahedral (Fig. 3c) nanoparticles are large and regular (111) planes as confirmed by the highly ordered FFT patterns (Fig. 3b and d, respectively). The 5-fold symmetry of planes direction and the clear boundary demonstrate the 5-fold twinned structure of nanoparticle (Fig. 3e), which is further confirmed by the 5-fold symmetrical FFT patterns (Fig. 3f).

The $Pd–Pt/C–NH_3$ catalysts with low Pt content exhibit comparable ORR catalytic activity to the commercial Pt/C (TKK Corp., Japan, denoted as TKK Pt/C). As shown in Fig. 4a and Table 1, the half-wave potential of $Pd_9Pt/C–NH_3$, $Pd_6Pt/C–NH_3$ and $Pd_4Pt/C–NH_3$ catalysts with low Pt content are 781, 791 and 800 mV, respectively, close to that of TKK Pt/C (811 mV). The superior ORR activity of $Pd–Pt/C–NH_3$ with low Pt content may be attributed to the more exposed regular (111) planes [8], the higher ratio of metallic form and the surface enrichment of Pt atoms, which will be discussion in detail in Section 3.3.

Due to the low Pt content and the inactivity of Pd for the MOR in acid solutions [16], the Pd–Pt/C catalysts exhibit excellent methanol tolerance. As shown in Fig. 4b and Table 1, the overpotentials (η) at 1 mA cm^{-2} caused by 0.5 M methanol are 19, 19 and 164 mV, respectively, significantly lower than that of TKK Pt/C (298 mV). The excellent methanol tolerance is also confirmed by the lower MOR activity of Pd–Pt/C catalysts. As shown in Fig. 5 and Table 1, the onset potentials of $Pd–Pt/C–NH_3$ for MOR are further higher than that of TKK Pt/C, while the peak current densities of $Pd–Pt/C–NH_3$ for MOR are markedly lower than that of TKK Pt/C. The higher onset

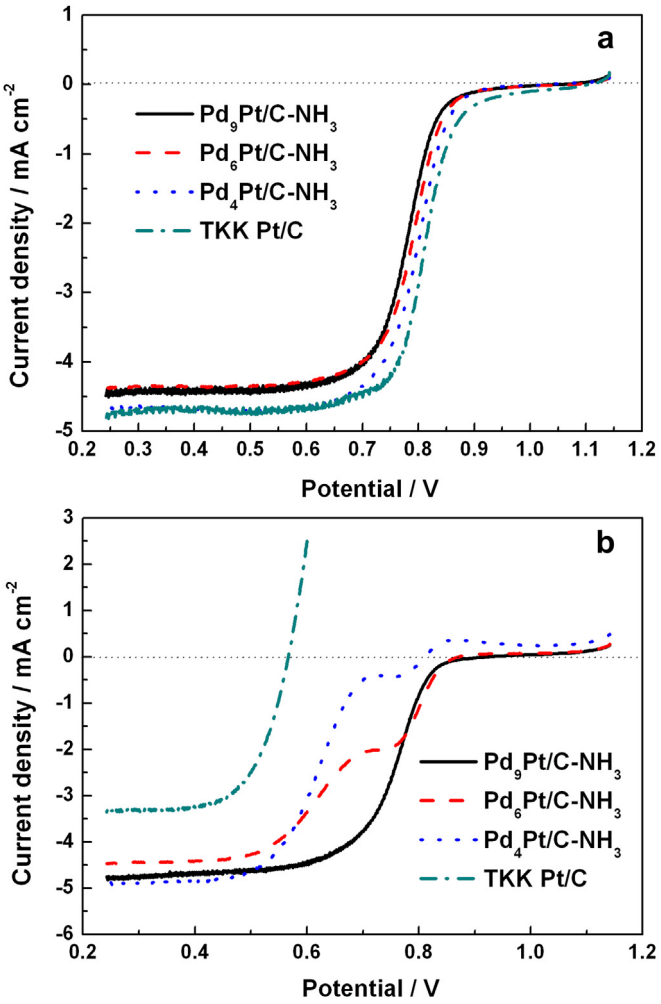

Fig. 4. ORR curves of Pd–Pt/C–NH_3 and TKK Pt/C catalysts in O_2 saturated 0.5 M H_2SO_4 without (a) and with 0.5 M CH_3OH (b). Scan rate of potential: 5 mV s^{-1}, rotational rate of RDE: 1600 rpm.

potential and lower peak current density indicate the lower MOR catalytic activity of Pd–Pt/C–NH_3 catalysts. Furthermore, the decreased onset potentials and increased peak current density of Pd–Pt/C–NH_3 with the increase of Pt content imply that the excellent methanol tolerance of Pd–Pt/C–NH_3 is attributed to the low Pt content.

3.2. Effects of ammonia complexation on the morphology of polyhedral Pd–Pt nanocrystalline

To understand the effect of ammonia complexation on the morphology and the mechanism for the formation of polyhedral Pd–Pt nanocrystallines, the Pd_6Pt/C–NH_3–N_2 catalyst was

Table 1
Electrochemical data of Pd–Pt/C–NH_3 and TKK Pt/C catalysts calculated from electrochemical measurements (Figs. 4 and 5).

	Pd_9Pt/C–NH_3	Pd_6Pt/C–NH_3	Pd_4Pt/C–NH_3	TKK Pt/C
Half-wave potential/V	0.781	0.791	0.800	0.811
η caused by methanol/V	0.019	0.019	0.164	0.298
Onset potential for MOR/V	0.60	0.59	0.59	0.40
Peak i for MOR/mA cm^{-2}	2.18	2.67	6.32	32.6

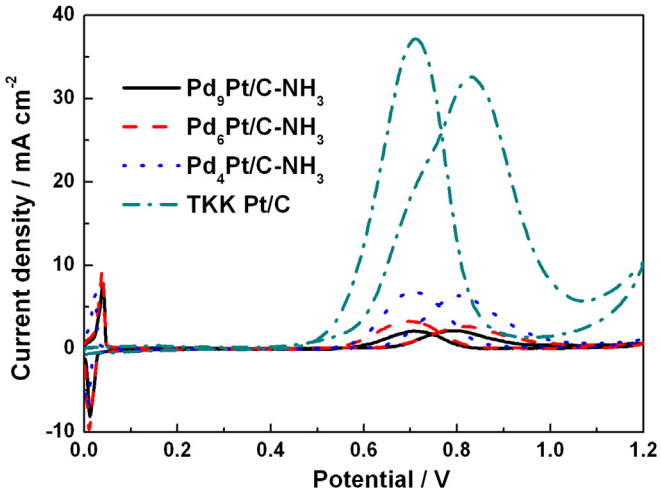

Fig. 5. MOR curves of Pd–Pt/C–NH_3 and TKK Pt/C catalysts in N_2 saturated 0.5 M H_2SO_4 with 0.5 M CH_3OH. Scan rate of potential: 5 mV s^{-1}.

obtained with ammonia solution as complexing reagent and using only N_2 as protective gas. Moreover, Pd_6Pt/C–EG was obtained using the conventional ethylene glycol method without ammonia in solution and without protective gas. These two Pd_6Pt/C catalysts were compared to Pd_6Pt/C–NH_3, which was obtained with ammonia solution as complexing reagent with NH_3 + N_2 as the protective gas. The preparation processes in detail of the three Pd_6Pt/C catalysts are described in Experimental section. Fig. 6 shows the TEM images of the Pd_6Pt/C catalysts. As shown, larger numbers of polyhedral (mainly tetrahedral and octahedral) metal nanoparticles are observed in the Pd_6Pt/C–NH_3 catalyst. Because of the complexation of ammonia in the Pd precursor solution, polyhedral shapes also appeared in the Pd_6Pt/C–NH_3–N_2 catalyst. However, the amount of polyhedron was less, and the morphology was less well defined because the protective gas was only N_2. Only spherical particles were observed in the Pd_6Pt/C–EG nanoparticles because of the absence of ammonia during the entire preparation process of the catalyst, thus confirming that the ammonia plays a key role on the nucleation of polyhedral seeds.

Although the data acquired thus far are insufficient to establish the mechanistic detail of the formation of polyhedral nanoparticles, we can propose a mechanism with the observed behaviors as follows: the slow reduction kinetics of Pd precursor, caused by the complexation between Pd^{2+} and ammonia, and the adsorption of ammonia on the surface of the polyhedral seeds may be attributed to the formation of polyhedral nanocrystallines. $Pd[(NH_3)_4]^{2+}$ formed from the reaction (Eq. (2)) increases the activation energy of Pd^{2+} reduction and slows down the reduction kinetics [17]. The slow reduction kinetics may result in more regular particle morphology and larger particle sizes. These can be confirmed by the order of metal particles size, the regularity extent of the particle shapes observed by TEM (Fig. 6) and the nanocrystalline sizes calculated from XRD patterns (Fig. 6d). As shown in Fig. 6, the metal particle size and shape regularity extent of nanoparticles obey the order of Pd_6Pt/C–NH_3 > Pd_6Pt/C–NH_3–N_2 > Pd_6Pt/C–EG. The crystalline sizes of Pd_6Pt/C–NH_3, Pd_6Pt/C–NH_3–N_2 and Pd_6Pt/C–EG calculated from Scherrer formula (Eq. (1)) are 10.1, 6.0, and 2.6 nm, respectively. Furthermore, as reported in Refs. [18,19], the adsorption of *N* atoms in the CTAB and PVP molecular on the nanocrystalline's surface, which controls the growth rates of different planes, plays important roles in the formation of polyhedral nanocrystallines. Therefore, the *N* atom of ammonia may play the similar roles in our synthesis of

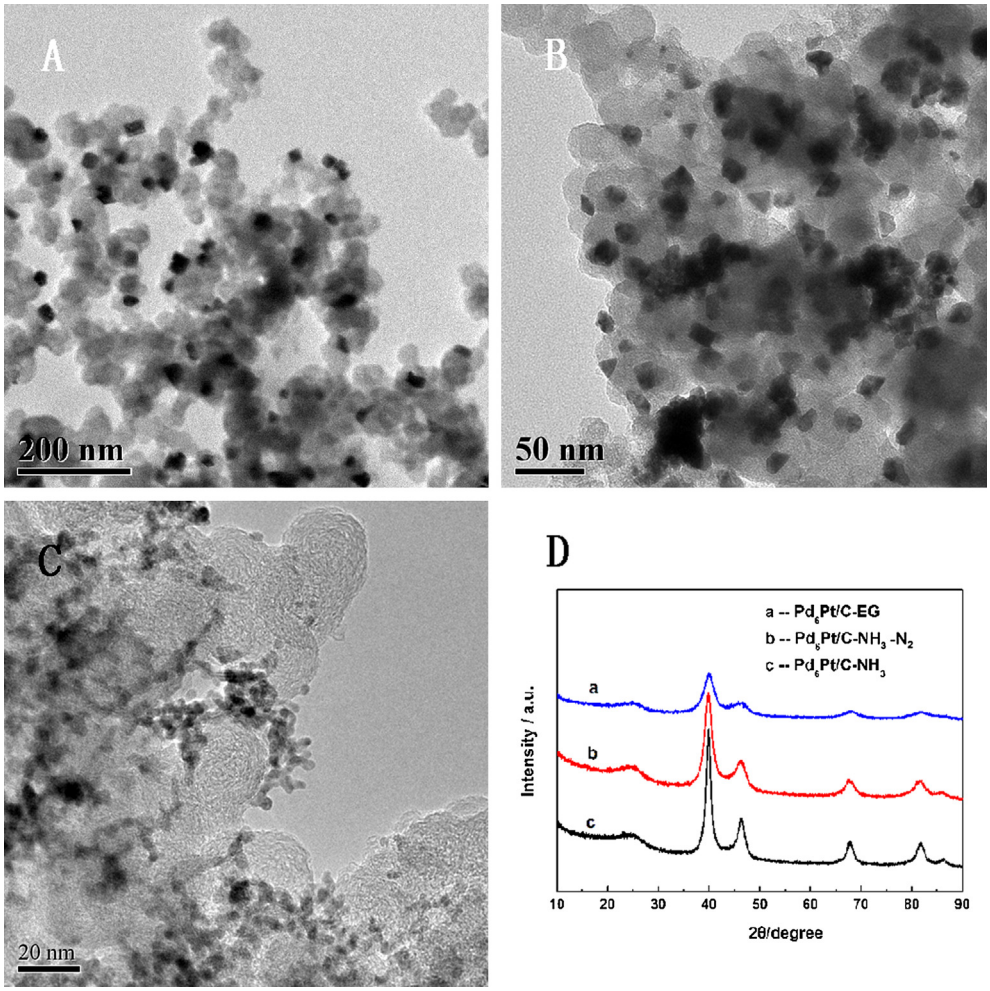

Fig. 6. TEM images of $Pd_6Pt/C{-}NH_3$ (A), $Pd_6Pt/C{-}NH_3{-}N_2$ (B), $Pd_6Pt/C{-}EG$ (C) catalysts and their XRD patterns (D).

polyhedral Pd–Pt nanoparticles. To sum up, the complexation of ammonia with Pd precursors and the adsorption of ammonia due to *N* atom play key roles in the formation of polyhedral Pd–Pt nanoparticles.

$$[PdCl_4]^{2-} + 4NH_3 \rightarrow [Pd(NH_3)_4]^{2+} + 4Cl^- \quad (2)$$

3.3. *Effect of polyhedral structures on the catalytic activity for ORR*

Electrochemical measurements combined with the HRTEM and XPS analysis were used to investigate the effect of metallic nanoparticles shape on its electrocatalytic activity for ORR. Generally, larger nanoparticles exhibit lower electrochemical surface area (ECSA). In this context, the order of particle sizes of Pd_6Pt/C catalysts prepared by different methods can be confirmed by cyclic voltammetry (CV) curves. Although the ECSA of the catalysts cannot be calculated quantitatively by the equation reported in the literature [20] due to the high Pd content in the Pd_6Pt/C catalysts, the ECSA of the Pd_6Pt/C catalysts can be compared qualitatively by the integral area of H adsorption/desorption peaks of the CV curves [21]. As shown in Fig. 7, the integral area of H adsorption/desorption peaks in the CV curves of $Pd_6Pt/C{-}NH_3$ catalyst is only half of that in $Pd_6Pt/C{-}EG$ catalyst, which means that the ECSA of $Pd_6Pt/C{-}NH_3$ catalyst is only half of that of $Pd_6Pt/C{-}EG$. However, the former exhibits better ORR activity than the latter. Fig. 8 shows the ORR curves of Pd_6Pt/C prepared by different methods. The mass activities of $Pd_6Pt/C{-}NH_3$, $Pd_6Pt/C{-}NH_3{-}N_2$, and $Pd_6Pt/C{-}EG$ at 0.85 V are 3.83, 4.66, and 2.82 mA mg^{-1} metals, respectively.

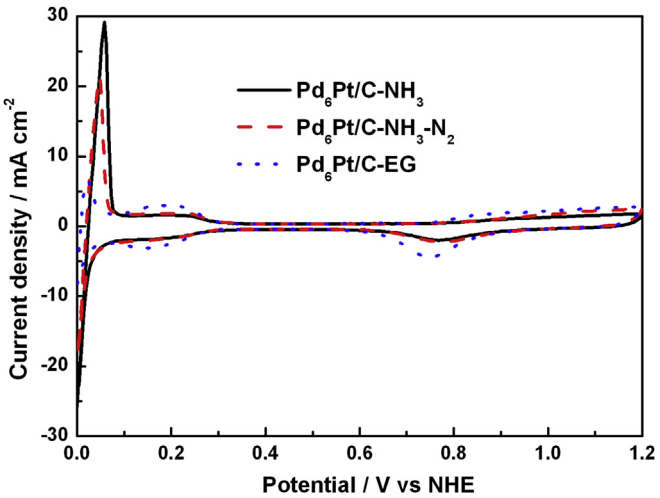

Fig. 7. CV curves of the Pd_6Pt/C prepared by different processes in N_2 saturated 0.5 M H_2SO_4 solution. Scan rate of potential: 50 mV s^{-1}.

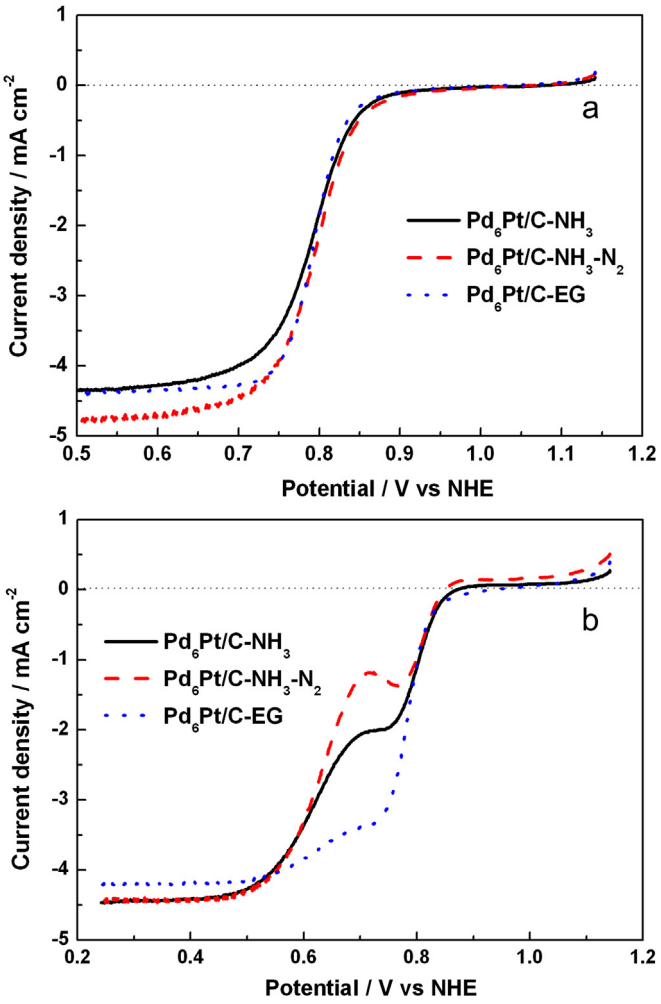

Fig. 8. ORR curves of the Pd_6Pt/C catalysts prepared by different processes in O_2 saturated 0.5 M H_2SO_4 solution without (a) and with 0.5 M CH_3OH (b). Scan rate of potential: 5 mV s^{-1}; rotational rate of RDE: 1600 rpm.

Compared to Pd_6Pt/C–EG with spherical Pd–Pt nanoparticles, Pd_6Pt/C–NH_3 and Pd_6Pt/C–NH_3–N_2 catalysts with polyhedral Pd–Pt nanoparticles show 1.36-fold and 1.65-fold mass specific activity, whereas their ECSA is much lower. Moreover, all the Pd_6Pt/C catalysts reveal excellent methanol tolerance (Fig. 8b) due to the low content of Pt in the catalysts. The superior ORR activity of the Pd_6Pt/C–NH_3 and Pd_6Pt/C–NH_3–N_2 catalysts may be attributed to their more exposed regular (111) planes of polyhedral nanoparticles [22]. For contrast, HRTEM image and FFT plots of Pd_6Pt/C–EG catalyst are shown in Fig. 9. As shown in HRTEM image, the exposed planes of the Pd_6Pt/C–EG catalyst are irregular and many (200) planes are observed. The diffraction circle observed in the FFT pattern confirms the irregular crystalline of the nanoparticles (Fig. 9b).

Table 2
Relative intensities of surface species and Pt/Pd ratios in the Pd_6Pt/C–NH_3, Pd_6Pt/C–NH_3–N_2 and Pd_6Pt/C–EG catalysts from XPS data.

Sample	Species	Relative intensity (%)	Species	Relative intensity (%)	Pd/Pt ratio
Pd_6Pt–NH_3	Pd^0	78.9			0.45
	Pd^{2+}	12.5			
	Pd^{4+}	8.6			
			Pt^0	67.5	
			Pt^{2+}	20.6	
			Pt^{4+}	11.9	
Pd_6Pt–NH_3–N_2	Pd^0	60.3			0.57
	Pd^{2+}	31.1			
	Pd^{4+}	8.6			
			Pt^0	57.0	
			Pt^{2+}	30.8	
			Pt^{4+}	12.2	
Pd_6Pt–EG	Pd^0	54.5			0.14
	Pd^{2+}	22.3			
	Pd^{4+}	23.2			
			Pt^0	64.5	
			Pt^{2+}	23.5	
			Pt^{4+}	12.0	

As we known, excessive adsorbed OH_{ads} groups block the active sites for O_2 adsorption, and thus depress the catalytic activity for ORR, whereas a higher ratio of metallic form is suitable for the desorption of the surface hydroxyl groups (OH_{ads}) and enhances the catalytic activity for ORR [23]. Moreover, the higher Pt/Pd ratio on the surface is also beneficial to improve the ORR activity [6,10]. Therefore, we also measured the surface metallic valence and Pt/Pd ratio on the Pd_6Pt/C catalysts by the XPS technique to investigate their effects. Table 2 shows the surface composition data of Pd_6Pt/C catalysts. The results show that the ratios of metallic Pd and Pt on the Pd_6Pt/C–NH_3 catalyst are up to 78.9% and 67.5%, while only 54.5% and 64.5% on the Pd_6Pt/C–EG catalyst. Furthermore, the surface Pt/Pd ratios of the Pd_6Pt/C–NH_3 (0.45) and Pd_6Pt/C–NH_3–N_2 (0.57) catalysts are markedly higher than those in Pd_6Pt/C–EG catalyst (0.14) and their precursors (0.17). These results are in good agreement with that the Pd_6Pt/C–NH_3, and the

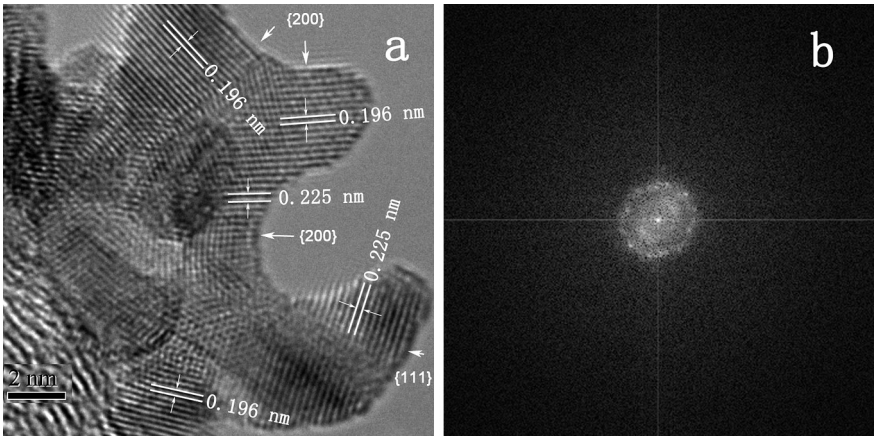

Fig. 9. HRTEM images (a) and the corresponding FFT plots (b) of the Pd_6Pt/C–EG catalyst.

$Pd_6Pt/C–NH_3–N_2$ catalysts exhibit superior ORR activities than $Pd_6Pt/C–EG$ catalyst.

4. Conclusions

In summary, we have developed a facile, surfactant-free strategy for synthesis of Pd–Pt electrocatalysts with polyhedral structures. The complexation of the Pd ion with ammonia and the appropriate Pd/Pt ratio, which results in suitable kinetics for nucleation and growth of metal nanoparticles, plays a key role in the formation of polyhedral nanoparticles. The Pd–Pt/C catalysts with polyhedral structures exhibit comparable ORR activity to commercial Pt/C catalysts and exhibit excellent methanol tolerance. The $Pd_6Pt/C–NH_3–N_2$ catalyst with polyhedral structures possesses 1.56-fold higher mass activity for ORR than its sphere-shaped $Pd_6Pt/C–EG$ counterpart, even though its ECSA is only half of the latter. The structure-dependent ORR activity was investigated using electrochemical measurements combined with HRTEM and XPS characterization. These results indicated that the superior activity may be attributed to the greater exposure of regular (111) planes, the higher ratio of metallic form and the surface enrichment of Pt atoms.

Acknowledgments

This work was supported by the National Natural Science Foundation of China (No. 51202213), Natural Science Foundation of Hebei Province (No. B2012203043) and China Postdoctoral Science Foundation (No. 2012M520597). Furthermore, this project was supported by the State Key Laboratory of Advanced Technology for Material Synthesis and Processing (Wuhan University of Technology) (No. 2013-KF-11).

References

[1] A.S. Aricò, S. Srinivasan, V. Antonucci, Fuel Cells 1 (2001) 133–161.
[2] X. Zhao, M. Yin, L. Ma, L. Liang, C. Liu, J. Liao, T. Lu, W. Xing, Energy Environ. Sci. 4 (2011) 2736–2753.
[3] K. Scott, W.M. Taama, P. Argyropoulos, K. Sundmacher, J. Power Sources 83 (1999) 204–216.
[4] M.-H. Shao, K. Sasaki, R.R. Adzic, J. Am. Chem. Soc. 128 (2006) 3526–3527.
[5] J.L. Fernandez, V. Raghuveer, A. Manthiram, A.J. Bard, J. Am. Chem. Soc. 127 (2005) 13100–13101.
[6] H. Li, G. Sun, N. Li, S. Sun, D. Su, Q. Xin, J. Phys. Chem. C 111 (2007) 5605–5617.
[7] E. Antolini, Energy Environ. Sci. 2 (2009) 915–931.
[8] Y.-W. Lee, A.R. Ko, D.-Y. Kim, S.-B. Han, K.-W. Park, RSC Adv. 2 (2012) 1119–1125.
[9] V. Mazumder, Y. Lee, S. Sun, Adv. Funct. Mater. 20 (2010) 1224–1231.
[10] B. Lim, M. Jiang, P.H.C. Camargo, E.C. Cho, J. Tao, X. Lu, Y. Zhu, Y. Xia, Science 324 (2009) 1302–1305.
[11] W. Niu, Z.-Y. Li, L. Shi, X. Liu, H. Li, S. Han, J. Chen, G. Xu, Cryst. Growth Des. 8 (2008) 4440–4444.
[12] X. Huang, N. Zheng, J. Am. Chem. Soc. 131 (2009) 4602–4603.
[13] N.V. Long, T. Asaka, T. Matsubara, M. Nogami, Acta Mater. 59 (2011) 2901–2907.
[14] B.E. Warren, X-ray Diffraction, Addison-Wesley, Reading, MA, 1969, pp. 251–254.
[15] Z. Liu, L.M. Gan, L. Hong, W. Chen, J.Y. Lee, J. Power Sources 139 (2005) 73–78.
[16] A. Capon, R. Parsons, J. Electroanal. Chem. 44 (1973) 239–254.
[17] H. Li, G. Sun, Q. Jiang, M. Zhu, S. Sun, Q. Xin, Electrochem. Comm. 9 (2007) 1410–1415.
[18] Y. Xiong, Y. Xia, Adv. Mater. 19 (2007) 3385–3391.
[19] B. Lim, Y. Xiong, Y. Xia, Angew. Chem. Int. Ed. 46 (2007) 9279–9282.
[20] A. Pozio, M. De Francesco, A. Cemmi, F. Cardellini, L. Giorgi, J. Power Sources 105 (2002) 13–19.
[21] H. Zhao, J. Yang, L. Wang, C. Tian, J. Jiang, H. Fu, Chem. Commun. 47 (2011) 2014–2016.
[22] C. Koenigsmann, A.C. Santulli, K. Gong, M.B. Vukmirovic, W.P. Zhou, E. Sutter, S.S. Wong, R.R. Adzic, J. Am. Chem. Soc. 133 (2011) 9783–9795.
[23] Z. Peng, H. Yang, J. Am. Chem. Soc. 131 (2009) 7542–7543.